A two-stage tropospheric correction model combining data from GNSS and numerical weather model

Jan Douša[1] · Michal Eliaš[1] · Pavel Václavovic[1] · Kryštof Eben[2] · Pavel Krč[2]

Abstract

We have developed a new concept for providing tropospheric augmentation corrections. The two-stage correction model combines data from a Numerical Weather Model (NWM) and precise ZTDs estimated from Global Navigation Satellite System (GNSS) permanent stations in regional networks. The first-stage correction is generated using the background NWM forecast only. The second-stage correction results from an optimal combination of the background model data and GNSS (near) real-time tropospheric products. The optimum correction is achieved when using NWM for the hydrostatic delay modeling and for vertical scaling, while GNSS products are used for correcting the non-hydrostatic delay. The method is assessed in several variants including study of the combination of NWM and GNSS data, spatial densification of the original NWM grid, and GNSS ZTD densification using tropospheric linear horizontal gradients. The first-stage correction can be characterized by overall accuracy of about 10 mm for ZTD (1-sigma). The second-stage correction supported with GNSS tropospheric products improved the first-stage correction by a factor of 2–4 in terms of the ZTD accuracy and by a factor of 2.5 in terms of its spatio-temporal stability.

Keywords GNSS · Tropospheric corrections · Zenith path delay · Numerical weather forecast · Precise point positioning

Introduction

Precise modeling of the refraction due to the neutral atmosphere is required for high-accurate applications of Global Navigation Satellite Systems (GNSS). The corresponding signal correction, called a tropospheric delay for GNSS, reaches about 2.3 m for a signal path from a satellite in the zenith to a ground receiver, and tens of meters when the satellite is close to the horizon. Such tropospheric delay needs

✉ Jan Douša
  jan.dousa@pecny.cz

[1] NTIS, New Technologies for the Information Society, Geodetic Observatory Pecný, RIGTC, Ústecká 98, 250 66 Zdiby, Czech Republic

[2] Institute of Computer Science, Academy of Sciences Czech Republic, Pod Vodárenskou věží 271/2, 182 07 Praha, Czech Republic

to be known with a sub-centimeter accuracy when using an autonomous method such as Precise Point Positioning (PPP) (Zumberge et al. 1997), or when processing data from two or more remote GNSS stations in a differential mode (Leick et al. 2015). The GNSS tropospheric delay is usually modeled using a station time-dependent parameter, the Zenith Total Delay (ZTD), which represents a sum of the Zenith Hydrostatic Delay (ZHD) and the Zenith Wet Delay (ZWD), according to their physical meaning. The zenith delays are projected into tropospheric path delays of signals from individual satellites using empirical mapping functions (Böhm et al. 2006a). In most cases of precise GNSS analysis, the ZTD is estimated as an unknown parameter from GNSS data, and when using PPP, the solution needs some time to converge.

A majority of real-time positioning and navigation applications either neglect the tropospheric effect, e.g. in low-accuracy applications, eliminate the effect using differential processing methods, or reduce the effect by corrections from standard models hardwired in the receiver. The accuracy of ZTD from the standard empirical models is limited to about 35 mm due to a two-dimensional representation and inaccurate modeling in the + temporal domain (Collins

and Langley 1998; Schüler 2013; Böhm et al. 2015; Dousa et al. 2015a). None of the above approaches can support PPP which is considered as a promising method for autonomous precise positioning applications, in particular when exploiting data from all available GNSS constellations, new signals and frequencies. With increasing accuracy of GNSS observations, models and products, the tropospheric effect remains one of the major sources of errors in PPP and can be reduced neither by advanced processing methods nor using additional data observed in situ.

Supported by new satellite data and high-performance computing facilities, Numerical Weather Models (NWM) are being steadily improved in terms of accuracy and spatial resolution. The actual state of the atmosphere, represented with three-dimensional data fields in time resolution of 1–6 h, is able to provide the ZTD with an accuracy of about 8–12 mm (Böhm et al. 2006b; Dousa et al. 2015a; Lu et al. 2016), which is by a factor of 3 more accurate than any standard model. The precision of ZTD prediction can be additionally characterized by a decrease of 1–2 mm per 6 h in a forecast horizon (Dousa et al. 2015b).

On the other hand, the ZTD can also be estimated from GNSS data when using geodetic receivers and precise satellite orbits, clocks, and other models in the post-processing regime with a precision of 2–4 mm, e.g. the final global product of the International GNSS Service, IGS, http://www.igs.org/products (Byram et al. 2011) or regional reanalysis such as recent EUREF 2nd reprocessing (Pacione et al. 2017). Actually, there is no alternative compared to the post-processing estimation of tropospheric parameters along with other GNSS parameters. Since 2000, the ZTD has been also estimated with a latency of 1 h and the accuracy of 4–7 mm using PPP (Gendt et al. 2004) or using the double-difference method for regional CORS networks (Ge et al. 2000; Douša 2001; van der Marel et al. 2004; Karabatic et al. 2011; Bosy et al. 2012) or global network (Dousa and Bennitt 2013). Such analyses aimed at supporting the assimilation of ZTDs into the NWM (De Pondeca and Zhou 2001; Cucurull et al. 2004; Vedel and Huang 2004). With the availability of real-time precise orbit and clock products of the IGS Real-Time Service, RTS, http://rts.igs.org (Caissy et al. 2012), the ZTD can be now estimated with real-time PPP reaching a precision of 5–9 mm (Li et al. 2014; Dousa and Vaclavovic 2014), i.e. slightly worse due to a lower quality of real-time global products. However, the estimation of the ZTD along with other parameters within a GNSS kinematic application becomes problematic due to its high correlation with receiver height, clock offsets, and ambiguities. This was practically demonstrated for the vertical positioning of a hot-air balloon (Vaclavovic et al. 2017).

The development of an optimal tropospheric correction model for real-time applications thus remains a challenging task, even while exploiting external data from NWM

predictions, GNSS CORS networks or in situ observed meteorological parameters. The assessment of accuracies of tropospheric corrections using NWM analysis, in situ observations and combining both of them, was performed by Krueger et al. (2004) and Dousa et al. (2015a). Other approaches have been recently developed to correct for the tropospheric effects for real-time PPP applications. Lu et al. (2016) used a priori NWM corrections further improved when using GNSS data. Other models used synoptic meteorological data collocated with GNSS CORS ZTDs (Wilgan et al. 2017; Hadas et al. 2013). Empirical models were developed based on GNSS CORS networks and without using NWM at all (Shi et al. 2014; Oliveira et al. 2017). The main disadvantages of all these methods can be summarized as follows: (a) precise vertical scaling is not possible for ZHD and ZWD without knowing an actual profile of meteorological data from NWM. Thus spatial parameter interpolation cannot be applied rigorously in a complex terrain, (b) ZWD cannot be separated from ZHD without observing atmospheric pressure accurately in situ or at a nearby synoptic station, (c) prediction of the ZHD and the ZWD is not possible from GNSS and, (d) GNSS-driven ZTD correction strongly depends on the availability of CORS networks and on the quality of (near) real-time ZTDs from GNSS analysis.

To overcome the above-mentioned problems, we introduce a two-stage correction model which aims at exploiting the synergy of two external input data sources—NWM and GNSS. The first stage of the model represents a background NWM-driven model and the second stage improves the ZWD by combining NWM and GNSS data. The principles of the new two-stage tropospheric correction model are introduced, and methods applied in both stages of the model are described. This method was used in four case studies and assessed focusing on aspects of further model optimizations. In the end, results are summarized, and optimal usage of the method in real-time positioning is discussed.

Principles of the two-stage model of tropospheric corrections

The two-stage correction model aims at optimal modeling and predicting hydrostatic and wet tropospheric corrections for real-time applications. The basic idea recalls the method of assimilation of GNSS ZTD into the NWM for the purpose of a numerical weather forecast (Vedel and Huang 2004; Poli et al. 2007; Bennitt and Jupp 2012). However, our approach focuses on GNSS user parameters and thus applies a simple method of combination of GNSS and NWM data.

First-stage correction based on the NWM

The first (background) correction stage is represented by the augmentation tropospheric model developed at Geodetic Observatory Pecný, GOP (Dousa et al. 2015a) which provides estimated parameters derived from NWM forecasts. First, the ZHD is numerically integrated from NWM profile or, alternatively, it can be calculated with a 1 mm accuracy from the surface atmospheric pressure (Saastamoinen 1972). Second, the surface temperature and the temperature lapse rate are estimated using linear regression from NWM profiles for the modeling of pressure-height vertical dependence. Third, the ZWD parameter is numerically integrated and its decay rate fitted from NWM profiles as suggested by Dousa and Elias (2014). Since the ZHD depends on the atmospheric pressure, it is rather stable in time and space and can be accurately predicted using NWM data (Vedel et al. 2001). The ZWD depends on temperature and water vapor pressure and is more difficult to model and predict because it changes rapidly with the distribution of atmospheric constituents along the signal line-of-sight (Askne and Nordius 1987).

Figure 1 shows the first-stage model (blue box), input NWM (red box), interpolation procedure (gray box) for the calculation of corrections at user position (green box), and additional procedures of generating the second-stage correction (yellow boxes) if input ZTDs from a regional network are available. All the parameters of the first-stage model, i.e. ZHD and ZWD plus auxiliary parameters for vertical scaling are estimated from the NWM forecast by using profiles of original meteorological parameters: atmospheric pressure, temperature and specific humidity. The GOP model, including parameters for vertical modeling, is derived for the NWM orography and grid resolution. Users can interpolate then ZHD and ZWD parameters to altitudes up to 10 km at any location within the region of interest.
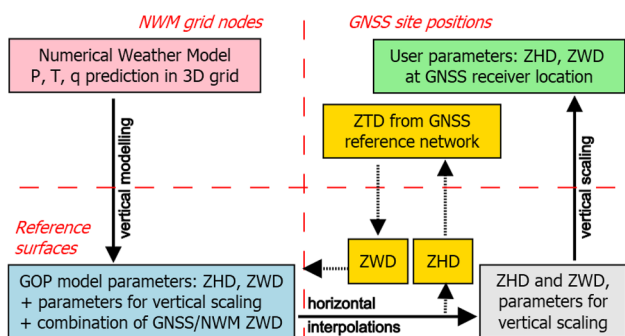
Fig. 1 Scheme of the two-stage combined tropospheric model. The second-stage is represented by yellow boxes additionally introduced on top of the first-stage represented by all other boxes

Second-stage correction improves ZWD estimation using GNSS data

The second-stage correction aims at improving the first-stage ZWD by exploiting GNSS precise tropospheric estimates provided by the CORS networks. For this purpose, we have developed a combination method of GNSS data with the parameters from the first model stage. The GNSS ZTD is assumed to improve mainly the non-hydrostatic contribution, similarly as in case of assimilating ZTDs into NWM. Therefore, ZWD at the locations of CORS stations which enters the processing of the second stage will be obtained by subtracting the first-stage ZHD from GNSS ZTD. It should be noted that GNSS ZWD estimates represent the highest accuracy for a complementary part of the ZHD to the ZTD. The ZHD from the first stage should be thus optimally used as a priori ZHD in the GNSS analysis.

The estimated CORS ZTDs need to be transformed to the model grid and combined with the output of the first-stage model. The second-stage correction procedure consists of the following steps:

1. bilinear interpolation of the first-stage model parameters to all CORS locations
2. retrieving ZWDs at the GNSS sites by subtracting the first-stage ZHD from GNSS ZTD:

$$\text{ZWD}_{\text{GNSS}|\text{site}} = \text{ZTD}_{\text{GNSS}|\text{site}} - \text{ZHD}_{\text{NWM}|\text{site}} \quad (1)$$

3. scaling ZWDs from station altitudes to a common reference surface using the tropospheric model parameters at site locations:

$$\text{ZWD}_{\text{GNSS}|\text{site}|\text{msl}} = \text{ZWD}_{\text{GNSS}|\text{site}} \left[1 + \frac{\beta H_{\text{site}|\text{msl}}}{T_{\text{GNSS}|\text{site}}} \right]^{\frac{(\gamma+1)g_m}{R_d \beta}}, \quad (2)$$

where γ is the ZWD decay parameter, $H_{\text{site}|\text{msl}}$ is the station height above the mean sea level, T is temperature and β its lapse rate, g_m is the mean gravity acceleration, and R_d is the gas constant for dry air

4. interpolating ZWDs horizontally from the stations onto the model grid at reference surface by means of a kriging method
5. scaling ZWDs at grid points from the reference surface to the model orography:

$$\text{ZWD}_{\text{GNSS}|\text{grid}} = \text{ZWD}_{\text{GNSS}|\text{grid}|\text{msl}} \left[1 + \frac{\beta H_{\text{grid}|\text{msl}}}{T_{\text{NWM}|\text{grid}}} \right]^{\frac{R_d \beta}{(\gamma+1)g_m}}, \quad (3)$$

6. combining obtained ZWDs with those from the first model stage.

Finally, the corrections for a user location are calculated in accordance with the utilization of the first model stage.

Figure 2 shows all the processing steps used to generate both tropospheric correction stages and are indicated by numbers in red circles. Colored boxes then represent inputs, intermediate parameters, processing steps, model parameters and user corrections.

The method proposed for the second stage thus operates mainly with GNSS ZWDs, however, still utilizing the parameters from the first model stage for isolating the ZWD from the ZTD at each station, Eq. (1), and for vertical scaling of the ZWD between reference surface, station altitudes, and the model surface. The ZWD vertical scaling follows the GOP approach described in Dousa and Elias (2014), however, in the present case defining the mean sea level as the reference surface for the horizontal ZWD interpolation.

For the purpose of converting a GNSS product to a regular model grid, represented by step 4, we applied a kriging method (Cressie 1993). Kriging is a geostatistical interpolation method, where the spatial prediction of a variable is computed as a weighted arithmetic mean of values in irregularly spaced spatial sample points. Weights are optimized so as to obtain minimum error in interpolated values. We interpolated ZWDs from CORS locations to grid nodes with simple kriging (Webster and Oliver 2007). This method assumes a known mean and covariance function, which determines the weights similarly to linear regression:

$$\hat{z}(x) = \sum_{i=1}^{n} \lambda_i z(x_i) + \left(1 - \sum_{i=1}^{n} \lambda_i\right)\mu \qquad (4)$$

with n the number of sample points, $z(x_i)$ and $\hat{z}(x)$ the input and estimated ZWDs, respectively, λ_i the kriging weights and μ the known stationary mean which is assumed to be constant over the whole data domain and was calculated as the overall mean of data.

Using a high-rate GNSS product in near real-time, the second-stage model can provide the time resolution of the GNSS ZTD sampling in order of minutes, e.g., 5 min. Since the first-stage model has a time resolution of the NWM, which is usually 1–6 h, the second-stage model has to perform temporal interpolation of parameters from the first-stage model prior to the application of the procedure described above.

After obtaining the interpolated GNSS ZWD at the model grid, we can further combine the value with the original ZWD from the background model, i.e., from NWM. Instead of discarding the first-stage NWM-based values of ZWD as in step 6 of the proposed method, a natural generalization would be considering a weighted average of NWM-based and GNSS-based ZWDs. Four combination variants are studied when assessing the contributions of both data sources, NWM and GNSS.

Model development software and datasets used for evaluation

The concept of the two-stage correction model has been implemented using the G-Nut library developed for GNSS positioning at GOP (Vaclavovic et al. 2013). The G-Nut/Shu end-user application was originally implemented for the NWM-based tropospheric correction model for augmentation systems of precise positioning. We enhanced the application for the new two-stage model by including different weighting methods for ZWDs from NWM and GNSS data.

We used a GNSS dataset and two input NWM datasets for the development and validation of the method. The input GNSS ZTDs were estimated by GOP for the benchmark within the project 'Advanced Global Navigation Satellite Systems tropospheric products for monitoring Severe Weather Events and Climate' (Dousa et al. 2016b). The GNSS ZTDs represent the reference solution with the domain covering Central Europe and for the time period May–June, 2013. The reference ZTD solution was analyzed using the Bernese GNSS software (Dach et al. 2015) and the strategy developed for the GOP 2nd European reprocessing

Fig. 2 Scheme of generation of two tropospheric model stages. Different box colors indicate: data inputs (red), user corrections (green), model grid corrections (blue) and GNSS-based parameters to improve the second stage of the model (yellow). Numbers correspond to procedure steps described in the text
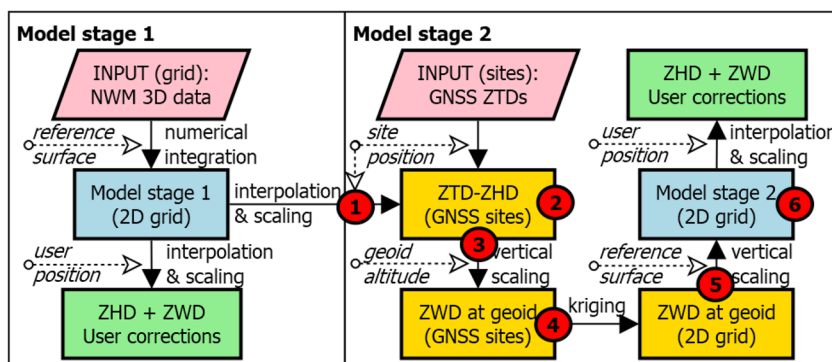
campaign (Dousa et al. 2017). The GNSS ZTDs and tropospheric horizontal gradients were estimated with a piecewise linear model and 1- and 6-h time resolution, respectively.

The two NWM datasets were selected so as to represent different types in terms of their scope, spatial resolution, and timeliness. The first is the ERA-Interim global homogeneous re-analysis (Dee et al. 2011) produced at the European Centre for Medium-Range Weather Forecasts (ECMWF). The ERA-Interim fields are available in synoptic times 00, 06, 12 and 18 UTC and have horizontal resolution of $1° × 1°$. The second dataset originated from an operational weather prediction actually used by GOP in operational tropospheric correction service supporting real-time precise positioning and navigation. Data fields with a $9 × 9$ km horizontal resolution and 1-h temporal resolution are forecasts produced by the mesoscale model WRF (Skamarock et al. 2008) operated by the Institute of Computer Science, Prague.

Evaluation and assessment of the two-stage correction

The performance of the proposed method was assessed at four test cases defined in Table 1. We evaluated (1) the benefit of the second-stage correction, (2) different variants of a combination of the two data sources using weighted averages of NWM and GNSS values, (3) the impact of increasing grid resolution, and (4) the effect of densification of GNSS ZTD data exploiting horizontal tropospheric gradients. Most experiments have been done for both NWM datasets.

Test case 1: evaluation of the proposed method, first-stage vs. second-stage correction

In this test case, all the available GNSS ZTDs were used as both input and control points. This is sometimes called a re-substitution test because the same data are used for both estimation and validation. The estimate of the error obtained in the re-substitution test is too optimistic, and its value may be viewed as a lower bound of error. Nevertheless, such a test is useful for comparison of first-stage vs. second-stage correction. Later in Test case 2, we provide error estimates

Table 1 Test cases for evaluating the proposed method and GNSS and NWM data combination

| Test case	Description
1	Comparison of first-stage and second-stage correction
2	Optimal ZWD combination from NWM and GNSS data
3	Impact of increasing grid resolution
4	GNSS ZTD densification exploiting horizontal tropospheric gradients

by means of cross-validation. Also, this test shows to which extent the method is able to recover the original values, and it can be viewed as a closed-loop test from original values via several approximations and interpolations back to them.

The procedure of the six steps above has been performed for the two background NWM datasets ERA-Interim and WRF-ICS. Summary statistics for this experiment are shown in Figs. 3 and 4. For the first-stage correction the overall systematic error and standard deviation reached $+ 2.6$ mm and 8.2 mm for the ERA-Interim background and $−0.8$ mm and 9.0 mm for the WRF-ICS background, respectively. The worse performance for the ERA-Interim in terms of systematic error is attributed to the low spatial resolution of the model and to additional errors due to spatial interpolations used between the model grid and station representations. On the other hand, the slightly worse performance of the WRF-ICS model in terms of standard deviation can be attributed to the non-null forecast horizon and to the routine operation mode. However, the long-term statistics over 6-h sessions generally indicate much higher variability in the NWM model performance when compared with GNSS ZTDs. For the second-stage correction the overall mean systematic error and standard deviation reached $+ 2.8$ and 4.4 mm for the ERA-Interim reanalysis, and $−0.2$ and 2.2 mm for the WRF-ICS model, respectively.

Despite several approximations, the results of the re-substitution test demonstrated that the proposed procedure works as expected. A significant portion of errors in the background NWM model has been corrected in the second
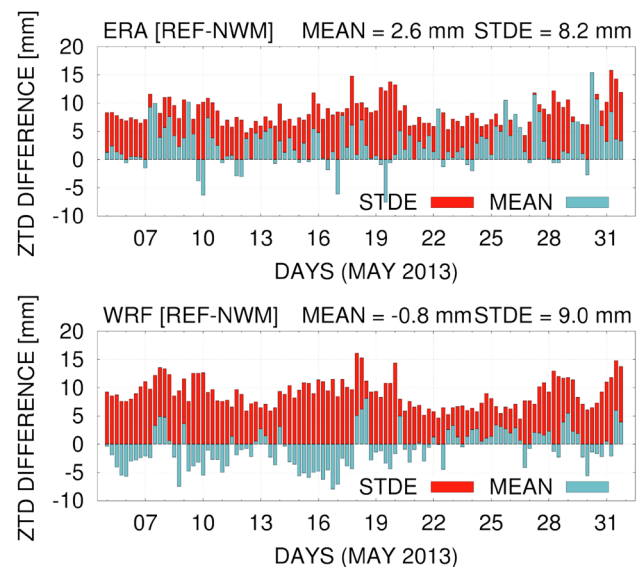
Fig. 3 Summary statistics of ZTD errors for the first-stage correction using a re-substitution method. Experiments performed with ERA-Interim background (top) and WRF-ICS (bottom) datasets for May 2013 and included 400 GNSS stations. REF: GNSS ZTDs at control points
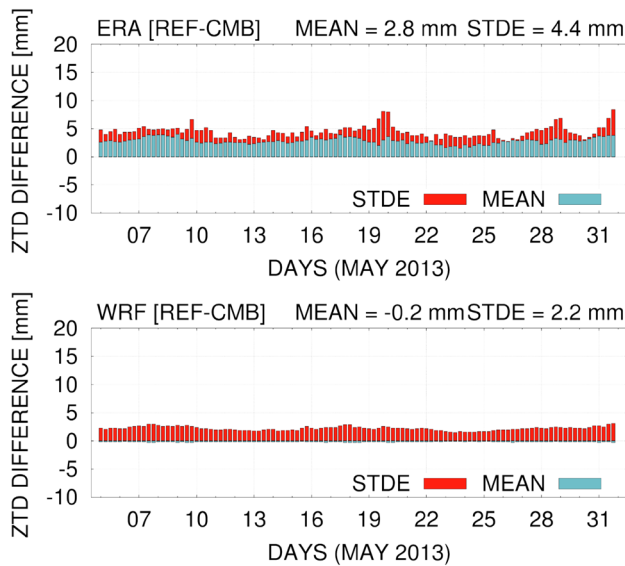
Fig. 4 Summary statistics of ZTD errors for the second-stage correction using a re-substitution method. Experiments performed with ERA-Interim background (top) and WRF-ICS (bottom) datasets for May 2013 and included 400 GNSS stations. REF: GNSS ZTDs at control points, CMB: NWM + GNSS combined ZTDs

stage. Errors in ZHD have also been absorbed by ZWD corrected values, while the error from such misinterpretation is considered as the second-order effect related only to height differences of grid points in the model reference surface. The two-stage model proved to be capable of providing highly accurate and very stable ZTD corrections for GNSS positioning.

Test case 2: combination of ZWD from GNSS and NWM data

As mentioned above, a natural generalization of step 6 of the proposed procedure would be considering a weighted average of NWM-based and GNSS-based ZWDs. Also, such an average may theoretically perform better than a GNSS-based ZWD if the number of GNSS stations is reduced. This test case investigates the properties of the weighted average at model grid nodes using a weighting in the form:

$$ZWD = \frac{ZWD_{GNSS} \cdot w_{GNSS} + ZWD_{NWM} \cdot w_{NWM}}{w_{GNSS} + w_{NWM}};$$
$$w_{NWM} = \frac{1}{\sigma_{NWM}^2}; \; w_{GNSS} = \frac{1}{\sigma_{GNSS}^2}, \quad (5)$$

where σ_{GNSS} and σ_{NWM} determine the accuracy of ZWD from GNSS and NWM, respectively. Table 2 introduces four variants (A–D) with different prescribed or estimated values of weights. The weighted average then represents the second-stage correction. The first-stage correction used as reference corresponds to the variant E.

Tables 3 and 4 summarize statistics of all differences between the original ZTD at a GNSS station and the estimated ZTD correction for the same station applying variants of weighted average at the grid nodes of ERA-Interim and WRF-ICS models. To test the performance of weighted average for reduced GNSS data, two spatial input data reduction variants are considered: 33.3% (R33) and 50.0% (R50). The omitted stations are selected randomly

Table 2 Combination variants of GNSS and NWM ZWDs

ID	ZWD variance (mm)	Description
A	$\sigma_{GNSS} = 10; \sigma_{NWM} \to \infty$	Only GNSS ZWD interpolated from surrounding stations
B	$\sigma_{GNSS} = 5; \sigma_{NWM} = 10$	NWM down-weighted with respect to GNSS
C	$\sigma_{GNSS} = \sigma_{KRIG}; \sigma_{NWM} = 10$	Variance from kriging used together with fixed NWM accuracy
D	$\sigma_{GNSS} = 10; \sigma_{NWM} = 10$	Equal contribution from NWM and GNSS
E	$\sigma_{GNSS} \to \infty; \sigma_{NWM} = 10$	Only ZWD from NWM, i.e., the first model stage

Table 3 Summary statistics of ZTD differences: GNSS − GNSS/ERA-Interim combination

Input data reduction	R0 or R100	R33	R50	R33 ǀ R50
Variant of weighting	Bias ± sdev (mm)	Bias ± sdev (mm)	Bias ± sdev (mm)	Improvement (% of sdev)
A (proposed, no NWM)	+2.8 ± 4.3	+2.4 ± 4.7	+2.7 ± 5.2	43.4 ǀ 35.8
B (NWM down weighted)	+2.8 ± 4.7	+2.5 ± 5.0	+2.7 ± 5.3	39.8 ǀ 34.6
C (kriging)	+2.8 ± 5.0	+2.4 ± 5.6	+2.7 ± 5.6	33.5 ǀ 30.9
D (equal weight)	+2.7 ± 5.9	+2.5 ± 6.0	+2.7 ± 6.0	27.7 ǀ 25.9
E (first stage)	+2.6 ± 8.2	+2.5 ± 8.3	+2.7 ± 8.1	-

Last column: improvement of standard deviation (sdev) with respect to the first-stage correction

Table 4 Summary statistics of ZTD differences: GNSS − GNSS/WRF-ICS combination

Input data reduction Variant of weighting	R0 or R100 Bias ± sdev (mm)	R33 bias ± sdev (mm)	R50 bias ± sdev (mm)	R33	R50 Improvement (% of sdev)
A (proposed, no NWM)	− 0.2 ± 2.2	− 0.5 ± 4.4	− 0.2 ± 4.7	49.4	45.9
B (NWM down weighted)	− 0.3 ± 2.7	− 0.5 ± 4.4	− 0.3 ± 4.6	49.4	47.2
C (kriging)	− 0.3 ± 2.7	− 0.8 ± 5.3	− 0.7 ± 5.7	39.0	34.5
D (equal weight)	− 0.6 ± 4.7	− 0.6 ± 5.4	− 0.5 ± 5.6	37.9	35.6
E (first-stage)	− 0.9 ± 8.9	− 0.8 ± 8.7	− 0.8 ± 8.8	–

Last column: improvement of standard deviation (sdev) with respect to the first-stage correction

and used for the evaluation (cross-validation). Additionally, the background model is referred to as R100 (with no GNSS data used) and the re-substitution as R0 (all input and control data).

Generally, all combination variants exploiting GNSS data showed better performances in terms of standard deviations compared to the background model. A positive impact of the GNSS is clearly visible in all variants while the best one utilized only GNSS data. An overall impact of the GNSS contribution in the combined model reached improvements in standard deviations, when compared to the first stage correction, from 36 to 46% (R50) and higher for the R33 input data reduction. Additionally, the variation of mean RMS in ZTD over all sessions within 1 month was reduced by a factor of 2.5 and more, namely from 2.80 to 1.10 mm for ERA-Interim and from 2.75 to 0.87 mm for WRF-ICS, when considering the R50 input data reduction.

Comparing the methods with re-substitution (R0) and independent (R33, R50) input and control data, the systematic error was not removed by using GNSS data in variants using ERA-Interim model. Improvement of the second model stage reached 48% (from 8.2 to 4.3 mm) in terms of standard deviation for the re-substitution test for ERA-Interim, while it resulted up to 75% (from 8.9 to 2.2 mm) improvement for WRF-ICS. Both limitations observed for ERA-Interim can be attributed to the sparse horizontal resolution of the global model. The improvements were, however, more similar when considering R33 reductions characterizing a higher impact of the input data reduction on the high-resolution model compared to the low-resolution one. An input data reduction (from 33 to 50%) then showed about a 7% degradation in the improvement which is small considering fewer input data. Interestingly, the reduction within the background model did not reveal any significant differences in the statistics indicating a homogeneity in the evaluation of different reductions. Although the horizontal resolution is significantly higher for WRF-ICS, its first stage correction resulted in a similar accuracy to ERA-Interim, which is

attributed to the 9–15-h prediction of the WRF-ICS within the operational forecast system.

Test case 3: impact of increasing grid resolution

The third test case aimed at studying the impact of the horizontal grid resolution on the ZWD combination. In this test, we used ERA-Interim data interpolated to higher horizontal resolutions than the original $1° × 1°$ grid. Certainly, we did not expect an improvement by interpolating the original NWM data to additional grid nodes, but in adding GNSS ZTDs from a dense GNSS network. This assumption was already supported by results achieved in the previous test case comparing statistics from NWM data having low/high resolution in combination with GNSS data in the second-stage model.

Figure 5 shows plots of systematic errors and standard deviations as a function of a densification factor of the NWM grid. The statistics are estimated by the re-substitution
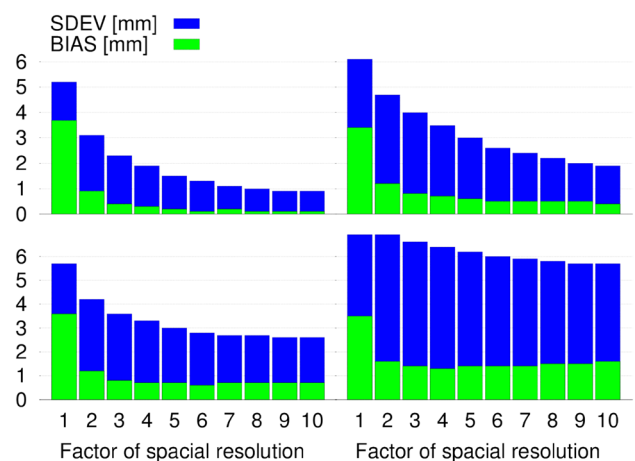
Fig. 5 Summary statistics of differences between NWM and GNSS ZTD using different ZWD weighting supported with an increased horizontal resolution of the ERA-Interim model. The ZWD combination A, B, C and D (from top-left to bottom-right) were studied on May 31, 2013, 00UTC

method as in Test case 1. The densification factor, on the x-axis in the figure, represents the increasing horizontal resolution of the original model grid. Each step from 1 to 10 represents an increase of horizontal resolution of the grid: 1—original resolution, 2—twofold densification (half size of the step), 3—three-fold, etc. The experiment has been performed for the four weighting variants from Test case 2, A, B, C, D (from top-left to bottom-right panel).

A fast decrease of ZTD systematic error to a sub-millimeter level can be observed by applying the first densification step (factor F = 2). Such grid corresponds to about 55 × 55 km in the horizontal resolution which is close to a mean distance between GNSS stations. The fast decrease of systematic errors indicates a high impact of the spatial densification on the quality of ZTD corrections when using GNSS data. ZTD standard deviations also decrease rapidly with the increasing densification factor, though less dramatically within the first one when compared to the systematic error.

Clearly, the variant A shows the largest decrease of the statistics demonstrating a full potential of contributions from GNSS to the two-stage correction and the benefit of increased horizontal resolution. Generally, when GNSS and NWM data were weighted in the ZWD combination, the impact of higher resolution on the statistics became lower. The variant D performed differently in the comparison—by averaging GNSS and NWM ZWDs revealed a minor improvement in terms of standard deviation thanks to a higher grid resolution and only partial improvement in terms of systematic error. As expected, variant E (not shown) disclosed even slightly worse statistics when only artificially increasing grid resolution of original NWM data.

Table 5 summarizes the statistics from the test case along with the original variant, i.e., without any densification (factor F = 1). By increasing the grid resolution, ZTD systematic errors and standard deviations approached the statistical results obtained with the WRF-ICS model (the last column in the table) observed for the variant A. We can notice slightly better result in terms of standard deviation for densified ERA-Interim model compared to the original WRF-ICS model. Generally, the comparison demonstrated a strong impact of GNSS on the ZWD weighted mean. In particular, higher resolution of the horizontal grid supports more optimal contributions from GNSS data. These are attributed to the non-hydrostatic component which dominates other locally specific characteristics. Also, a significant decrease of systematic errors was observed for ERA-Interim model when increasing the grid resolution. This indicates that GNSS ZTDs are able to correct the full ZTD effect, thus not only the non-hydrostatic component but also errors in the hydrostatic component but also errors in the hydrostatic component of the background NWM model if the grid resolution is dense enough to exploit optimally data from CORS network.

Test case 4: GNSS ZTD densification exploiting horizontal tropospheric gradients

The fourth test case aimed at testing an optimal utilization of GNSS tropospheric products if, in addition, horizontal tropospheric parameters are provided from a GNSS analysis. The idea is to improve the spatial resolution of the GNSS ZTDs when contributing to the combination with a high-resolution NWM model such as the WRF-ICS (9×9 km). For completeness, we have performed the experiment with the low-resolution ERA-Interim model ($1° \times 1°$) too.

We have implemented a method for calculation of pseudo-ZTD values using the parameters estimated at GNSS stations, namely ZTDs and horizontal gradients in North (G_N) and East (G_E) directions (Brenot et al. 2006). One pseudo-ZTD value was generated at 25 km distances from each original GNSS site in the azimuth of a maximum horizontal gradient. In this way, the number of input and control points has increased two times. A height of 12 km was used for the troposphere when calculating elevation angles. The pseudo-ZTDs were calculated using elevation angle (e) and azimuth (A) by the formula:

$$\overline{ZTD} = ZTD + 1/\tan(e) \cdot \left[G_N \cos(A) + G_E \sin(A) \right]. \quad (6)$$

The errors have been estimated by the re-substitution method and experiments have been performed for the weighting variants A and E. We did not distinguish between pseudo-ZTDs and ZTDs in the evaluation.

Table 5 Impact of increased ERA-Interim spatial resolution in the first-stage model

| Factor for increasing spatial resolution Variant ID	F = 1 (none) Bias ± sdev (mm)	F = 2 (twofold) Bias ± sdev (mm)	F = 3 (threefold) Bias ± sdev (mm)	F = 4 (fourfold) Bias ± sdev (mm)	WRF (none) Bias ± sdev (mm)
A (proposed, no NWM)	+2.8 ± 4.3	+0.6 ± 2.7	+0.3 ± 2.0	+0.2 ± 1.6	−0.2 ± 2.2
B (NWM down weighted)	+2.8 ± 4.7	+0.9 ± 3.7	+0.7 ± 3.2	+0.6 ± 2.9	−0.3 ± 2.7
C (kriging)	+2.8 ± 5.0	+1.0 ± 4.2	+0.8 ± 3.6	+0.6 ± 3.1	−0.3 ± 2.7
D (equal weight)	+2.7 ± 5.9	+1.4 ± 6.2	+1.3 ± 6.0	+1.2 ± 5.7	−0.6 ± 4.7
E (first stage)	+2.6 ± 8.2	+2.2 ± 10.5	+2.2 ± 10.7	+2.2 ± 10.6	−0.9 ± 8.9
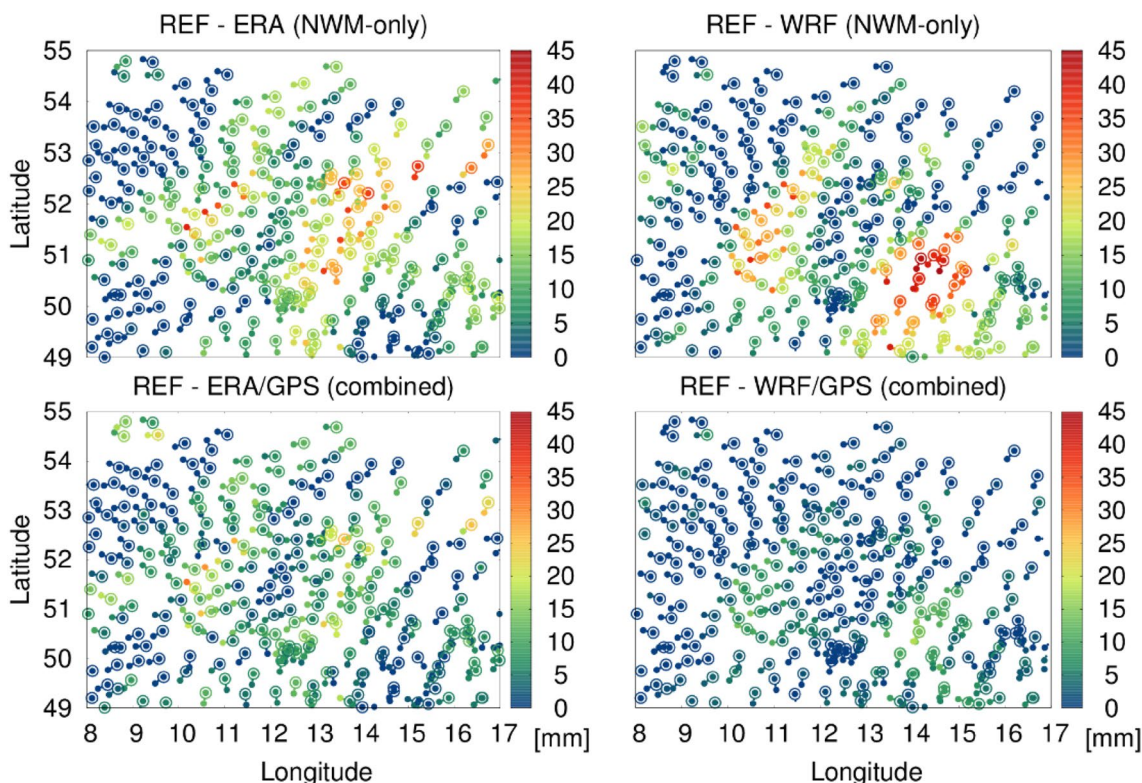
Fig. 6 Differences of ZTDs (circles with dots inside) and pseudo-ZTDs (dots connected to the circles) at the distance of 25 km with respect to the reference GNSS ZTDs. First-stage correction (top panels), the second-stage correction (bottom panels); ERA-Interim background (left panels), WRF-ICS background (right panels), May 31, 12 UTC, 2013

Figure 6 depicts sample results of the GNSS product densification, showing tuples of ZTD and pseudo-ZTD generated as described above and displayed by circles (with a small dot inside) and small dots (connected to the circles). Colors indicate differences with respect to the reference values stemming from the GNSS product. Two top panels display ZTD differences from the first-stage correction, while the bottom plots depict ZTD differences estimated by the second-stage correction. The underlying ERA-Interim and WRF-ICS models are shown in the left and right panels, respectively. Generally, the figure shows a good capability of deriving pseudo-ZTDs from GNSS ZTDs and horizontal gradients. With the densified GNSS network, the second-stage correction performs better for WRF-ICS background NWM compared to the ERA-Interim background. This occurs since the ERA-Interim grid is too coarse and the correction cannot fully benefit from a dense GNSS network.

Figure 7 then displays ZTD statistics over a month of the two-stage correction for the R33 input data reduction. The plots demonstrate an excellent performance over all 6-h sessions in terms of both accuracy and stability, similar to that observed when using the proposed method and all GNSS ZTDs. The results are comparable with the re-substitution
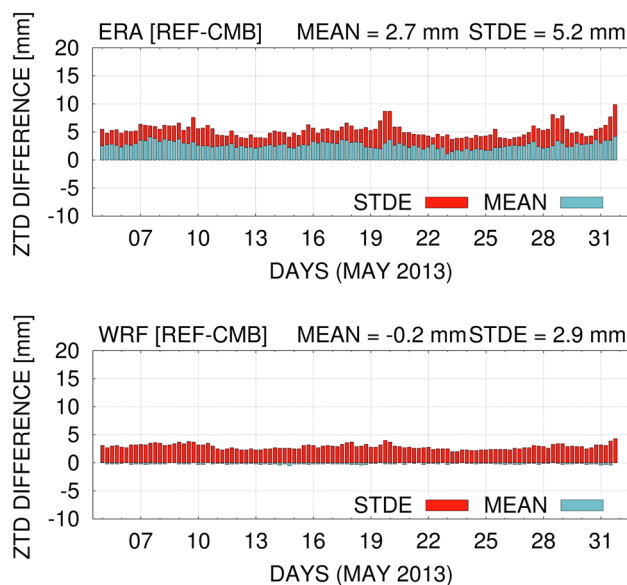
Fig. 7 Session mean statistics of two-stage model ZTD comparisons at GNSS sites using R33 reduction and original GNSS ZTDs as the reference; top: ERA-Interim; bottom: WRF-ICS

error, see Fig. 4. The ZTD standard deviation has decreased by 43% (from 9.3 to 5.3 mm) for ERA-Interim and by 76% (from 9.6 to 2.3 mm) for WRF-ICS when compared without input data reduction.

Table 6 summarizes results of the second-stage correction (variant A) and first-stage correction (variant E) with and without densification of the GNSS product. For a period of a month (May 2013) we report the statistics for both background NWM models and the two input data reduction variants, making no difference between pseudo-ZTDs and ZTDs in the evaluation.

The lower two rows of the table (variant E) show another evaluation of the first-stage correction: against the original values (identical to those of in Table 2) and against original pseudo-ZTD values. The degradation of standard deviations in the second row is due to errors introduced by approximations in the pseudo-ZTD calculation, including the assumptions such as the mean height of the troposphere, linear 'tilting' of the troposphere and optimal location of pseudo-ZTD. The effect can be seen mainly when comparing the values for second-stage correction and no input data reduction is used.

A clear improvement was however observed in case of WRF-ICS model in both R33 and R50 input data reduction, demonstrating the ability of gradients to compensate significantly the reduction of the number of GNSS stations. The improvement was from 4.7 to 3.0 mm for R50 and WRF-ICS reaching about 36% with respect to the solution using GNSS ZTDs only. It confirms again the benefit of using GNSS data in combination with NWM. GNSS ZTDs and tropospheric gradients are able to characterize the non-hydrostatic contribution from the troposphere accurately, stably and with a high temporal and spatial resolution.

Conclusions

We have developed a new theoretical concept of a two-stage tropospheric correction model, intended for GNSS precise real-time positioning applications. The model benefits from the synergy between NWM and GNSS data and enhances the original GOP augmentation model introduced in Dousa et al. (2015a). The first stage correction is derived from the background NWM forecast, and it is available always for the region of interest. The newly proposed second-stage correction is provided when tropospheric parameters from GNSS CORS network are available from the near real-time analysis. This optional stage provides accurate and stable ZWDs or, more precisely ZTDs when also correcting NWM-derived (first-stage) hydrostatic delay. Hence, the two-stage model provides a flexible correction based on the background model or combining it with additional GNSS tropospheric products from the CORS network analysis.

The concept was implemented in the G-Nut/Shu software for testing and assessing different variants of ZWD weighting method. The evaluation demonstrated that the new concept provides highly accurate and stable results despite several involved approximations. The GNSS data were able to improve significantly the non-hydrostatic part of the NWM-based tropospheric model but could also absorb errors in the hydrostatic component coming from the underlying NWM data. The second-stage model reached a significant improvement in terms of ZTD standard deviations, in total over 36–50%, when evaluated with products from independent GNSS stations. A decrease of systematic errors was also observed, though negligible in overall statistics. The highest impact of combining GNSS and NWM data has been seen in terms of the stability of ZTD, characterized by variation over all sessions, which improved the accuracy of ZTD by a factor of 2.5 and more.

The GNSS contribution to the two-stage correction model originates in the ability to reflect local phenomena where the model resolution plays a key role. Actually, the GNSS products (ZTDs) are assimilated into the tropospheric correction model. We demonstrated a fast decrease of the error statistics when simulating a higher horizontal resolution for the ERA-Interim model; comparable results have been then obtained to those from the high-resolution WRF-ICS model. Comparing several ZWD combination methods, optimal results were achieved simply by replacing the original NWM ZWDs with GNSS ZWDs if these were interpolated robustly to the model grid points.

Table 6 Summary statistics for ZTDs combined from GNSS and ERA-Interim/WRF-ICS data

NWM model	ERA-Interim			WRF-ICS		
Input data reduction	none (R100)	R33	R50	none (R100)	R33	R50
Variant	Bias ± sdev (mm)	Bias ± sdev (mm)	Bias ± sdev (mm)	Bias ± sdev (mm)	Bias ± sdev (mm)	Bias ± sdev (mm)
A (original-ZTDs)	+2.8±4.3	+2.4±4.7	+2.7±5.2	−0.2±2.2	−0.5±4.4	−0.2±4.7
A (pseudo-ZTDs)	+2.8±5.3	+2.7±5.2	+3.0±5.5	−0.2±2.4	−0.2±2.9	−0.0±3.0
E (original-ZTDs)	+2.6±8.2	+2.5±8.3	+2.7±8.1	−0.9±8.9	−0.8±8.7	−0.8±8.8
E (pseudo-ZTDs)	+2.6±9.3	+2.6±9.3	+2.7±9.4	−0.8±9.6	−0.7±9.5	−0.8±9.6

Using tropospheric horizontal gradients estimated for each GNSS station, we developed a method to calculate so-called pseudo-ZTDs to densify GNSS ZTD field. These pseudo values mimic values from real stations and can to some extent compensate a low number of GNSS stations available. This technique required a high-resolution NWM and performed well with the WRF-ICS background model. The combination of GNSS ZTDs and pseudo-ZTDs with NWM showed a 70% improvement in terms of standard deviations compared to the first-stage correction, and a 36% improvement compared to the second-stage correction applying a standard combination of NWM and GNSS ZTDs only.

The proposed method of NWM and GNSS data combination demonstrated high accuracy and stability over time. It is thus promising for implementing a new service for tropospheric corrections for real-time precise positioning.

References

Askne J, Nordius H (1987) Estimation of tropospheric delay for microwaves from surface weather data. Radio Sci 22(3):379–386. https://doi.org/10.1029/RS022i003p00379

Bennitt G, Jupp A (2012) Operational assimilation of GPS zenith total delay observations into the met office numerical weather prediction models. Mon Weather Rev 140(8):2706–2719. https://doi.org/10.1175/MWR-D-11-00156.1

Böhm J, Niell A, Tregoning P, Schuh H (2006a) Global mapping function (GMF): a new empirical mapping function based on numerical weather model data. Geophys Res Lett 33(7):L07304. https://doi.org/10.1029/2005GL025546

Böhm J, Werl B, Schuh H (2006b) Troposphere mapping functions for GPS and very long baseline interferometry from European Centre for Medium-Range Weather Forecasts operational analysis data. J Geophys Res 111:B02406. https://doi.org/10.1029/2005JB003629

Böhm J, Niell A, Tregoning P, Schuh H (2015) Development of an improved empirical model for slant delays in the troposphere (GPTw). GPS Solut 19(3):433–441. https://doi.org/10.1007/s10291-014-0403-7

Bosy J, Kaplon J, Rohm W, Sierny J, Hadas T (2012) Near real-time estimation of water vapour in the troposphere using ground GNSS and the meteorological data. Ann Geophys 30:1379–1391. https://doi.org/10.5194/angeo-30-1379-2012

Brenot H, Ducrocq V, Walpersdorf A, Champollion C, Caumont O (2006) GPS zenith delay sensitivity evaluated from high-resolution numerical weather prediction simulations of the 8–9 September 2002 flash flood over southeastern France. J Geoph Res 111(D15):D15105. https://doi.org/10.1029/2004JD005726

Byram S, Hackman C, Tracey J (2011) Computation of a high precision GPS-based troposphere product by the USNO. In: Proceedings ION GNSS 2011, Institute of Navigation, Portland, September 19–23, pp 572–578

Caissy M, Agrotis L, Weber G, Hernandez-Pajares M, Hugentobler U (2012) The International GNSS Real-Time Service. GPS World (June 1)

Collins JP, Langley RB (1998) The residual tropospheric propagation delay: how bad can it get? In: Proceedings ION GPS 1998, Institute of Navigation, Nashville, September 15–18

Cressie NAC (1993) Statistics for spatial data. Wiley series in probability and mathematical statistics: applied probability and statistics. Wiley, New York

Cucurull L, Vandenberghe F, Barker D, Vilaclara E, Rius A (2004) Three-dimensional variational data assimilation of ground-based GPS ZTD and meteorological observations during the 14 December 2001 storm event over the Western Mediterranean Sea. Mon Weather Rev 132:749–763. https://doi.org/10.1175/1520-0493(2004)1322.0.CO;2

Dach R, Lutz S, Walser P, Fridez P (eds) (2015) Bernese GNSS Software Version 5.2. User manual, Astronomical Institute. University of Bern, Bern Open Publishing, Bern

De Pondeca MSFV, Zhou X (2001) A case study of the variational assimilation of GPS Zenith Delay observations into a mesoscale model. J Clim Appl Meteorol 40:1559–1576

Dee DP, Uppala SM, Simmons AJ et al (2011) The ERA-Interim reanalysis: configuration and performance of the data assimilation system. Q J R Meteorol Soc 137:553–597. https://doi.org/10.1002/qj.828

Dousa J, Bennitt GV (2013) Estimation and evaluation of hourly updated global GPS zenith tropospheric delays over ten months. GPS Solut 17(4):453–464. https://doi.org/10.1007/s10291-012-0291-7

Dousa J, Elias M (2014) An improved model for calculating tropospheric wet delay. Geophys Res Lett 41(12):4389–4397. https://doi.org/10.1002/2014GL060271

Dousa J, Vaclavovic P (2014) Real-time zenith tropospheric delays in support of numerical weather prediction applications. Adv Space Res 53(9):1347–1358. https://doi.org/10.1016/j.asr.2014.02.021

Dousa J, Elias M, Veerman H, van Leeuwen SS, Zelle H, de Haan S, Martellucci A, Perez RO (2015a) High accuracy tropospheric delay determination based on improved modelling and high resolution Numerical Weather Model. In: Proceedings of ION GNSS 2015. Institute of Navigation, Tampa, September 14–18, pp 3734–3744

Dousa J, Vaclavovic P, Krc P, Elias M, Eben E, Resler J (2015b) NWM forecast monitoring with near real-time GNSS products. In: Proceedings of the 5th Scientific Galileo Colloquium, Braunschweig, October 27–29. http://old.esaconferencebureau.com/docs/default-source/15a08_session1/044-dousa.pdf?sfvrsn=2

Dousa J, Dick G, Kacmarik M, Brozkova R, Zus F, Brenot H, Stoycheva A, Möller G, Kaplon J (2016) Benchmark campaign and case study episode in central Europe for development and assessment of advanced GNSS tropospheric models and products. Atmos Meas Tech 9:2989–3008. https://doi.org/10.5194/amt-9-2989-2016

Dousa J, Vaclavovic P, Elias M (2017) Tropospheric products of the second European GNSS reprocessing (1996–2014). Atmos Meas Tech 10:1–19. https://doi.org/10.5194/amt-10-1-2017

Douša J (2001) Towards an operational near-real time precipitable water vapor estimation. Phys Chem Earth Part A 26(3):189–194. https://doi.org/10.1016/S1464-1895(01)00045-X

Ge M, Calais E, Haas J (2000) Reducing satellite orbit error effects in near real-time GPS zenith tropospheric delay estimation for meteorology. Geophys Res Lett 27(13):1915–1918

Gendt G, Dick G, Reigber C, Tomassini M, Liu YX, Ramatschi M (2004) Near real time GPS water vapor monitoring for numerical weather prediction in Germany. J Meteorol Soc Jpn 82(1B):361–370. https://doi.org/10.2151/jmsj.2004.361

Hadas T, Kaplon J, Bosy J, Sierny J, Wilgan K (2013) Near-real-time regional troposphere models for the GNSS precise point positioning technique. Meas Sci Technol 24(5):055003. https://doi.org/10.1088/0957-0233/24/5/055003

Karabatic A, Weber R, Haiden T (2011) Near real-time estimation of tropospheric water vapour content from ground based GNSS data and its potential contribution to weather now-casting in Austria. Adv Space Res 47:1691–1703. https://doi.org/10.1016/j.asr.2010.10.028

Krueger E, Schueler T, Hein GW, Martellucci A, Blarzino G (2004) Galileo tropospheric correction approaches developed within GSTB-V1. In: Proceedings of ENC-GNSS 2004, Rotterdam

Leick A, Rapoport L, Tatarnikov D (2015) GPS satellite surveying. 4th edn. Wiley, New York

Li X, Dick G, Ge M, Heise S, Wickert J, Bender M (2014) Real-time GPS sensing of atmospheric water 716 vapor: precise point positioning with orbit, clock and phase delay corrections. Geophys Res Lett 41(717):3615–3621. https://doi.org/10.1002/2013GL058721

Lu C, Zus F, Ge M, Heinkelmann R, Dick G, Wickert J, Schuh H (2016) Tropospheric delay parameters from numerical weather models for multi-GNSS precise positioning. Atmos Meas Tech 9:5965–5973. https://doi.org/10.5194/amt-9-5965-2016

Oliveira PS, Morel L, Fund F, Legros R, Monico JFG, Durand S, Durand F (2017) Modeling tropospheric wet delays with dense and sparse network configurations for PPP-RTK. GPS Solut 21(1):237–250. https://doi.org/10.1007/s10291-016-0518-0

Pacione R, Araszkiewicz A, Brockmann E, Dousa J (2017) EPN-Repro2: a reference GNSS tropospheric data set over Europe. Atmos Meas Tech 10:1689–1705. https://doi.org/10.5194/amt-10-1689-2017

Poli P, Moll P, Rabier F, Desroziers G, Chapnik B, Berre L, Healy SB, Andersson E, Guelai FZE (2007) Forecast impact studies of zenith total delay data from European near real-time GPS stations in Meteo France 4DVAR. J Geophys Res 112:D06114. https://doi.org/10.1029/2006JD007430

Saastamoinen J (1972) Atmospheric correction for the troposphere and stratosphere in radio ranging of satellites. The use of artificial satellites for geodesy, AGU, Washington DC. https://doi.org/10.1029/GM015p0247

Schüler T (2014) The TropGrid2 standard tropospheric correction model. GPS Solut 18(1):123–131. https://doi.org/10.1007/s10291-013-0316-x

Shi JB, Xu CQ, Guo JM, Gao Y (2014) Local troposphere augmentation for real-time precise point positioning. Earth Planets Space 66:30. https://doi.org/10.1186/1880-5981-66-30

Skamarock WC, Klemp JB, Dudhia J, Gill DO, Barker DM, Duda MG, Huang XY, Wang W, Powers JG (2008) A description of the advanced research WRF version 3. NCAR Technical Note NCAR/TN-475 + STR. https://doi.org/10.5065/D68S4MVH

Vaclavovic P, Dousa J, Gyori G (2013) G-Nut software library—state of development and first results. Acta Geodyn Geomater 10(4):431–436. https://doi.org/10.13168/AGG.2013.0042

Vaclavovic P, Dousa J, Elias M, Kostelecky J (2017) Using external tropospheric corrections to improve GNSS positioning of hot-air balloon. GPS Solut 21(4):1479–1489. https://doi.org/10.1007/s10291-017-0628-3

van der Marel H, Brockmann E, de Haan S, Douša J, Johansson J, Gendt G, Kristiansen O, Offiler D, Pacione R, Rius A, Vespe F (2004) COST-716 demonstration project for the near real-time estimation of integrated water vapour from GPS. Phys Chem Earth 29:187–199. https://doi.org/10.1016/j.pce.2004.01.001

Vedel H, Huang XY (2004) Impact of ground based GPS data on numerical weather prediction. Meteorol Soc Jpn 82:459–472

Vedel H, Mogensen KS, Huang XY (2001) Calculation of zenith delays from meteorological data comparison of NWP model, radiosonde and GPS delays. Phys Chem Earth (A) 26(6–8):497–502. https://doi.org/10.1016/S1464-1895(01)00091-6

Webster R, Oliver MA (2007) Geostatistics for environmental scientists. Statistics in practice. Wiley, New York

Wilgan K, Hurter F, Geiger A, Rohm W, Bosy J (2017) Tropospheric refractivity and zenith path delays from least-squares collocation of meteorological and GNSS data. J Geod 91(2):117–134. https://doi.org/10.1007/s00190-016-0942-5

Zumberge JF, Heflin MB, Jefferson DC, Watkins MM, Webb FH (1997) Precise point positioning for the efficient and robust analysis of GPS data from large networks. J Geophys Res 102:5005–5018

Jan Douša received his M.Sc. and Ph.D. degrees in geodesy from the Czech Technical University in Prague in 1995 and 1999, respectively. Since 1996, he has worked at Geodetic Observatory Pecný for developing high-accuracy GNSS applications including determination of precise orbits, modeling and monitoring troposphere, the realization of the reference frame and others. He is a founder and developer of the G-Nut software library and end-user applications.
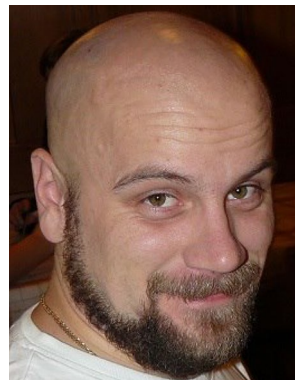
Michal Eliaš received his M.Sc. degree in geodesy at the Czech Technical University in Prague in 2010, and he is a Ph.D. candidate there. Since 2012, he has worked at the Geodetic Observatory Pecný with research focuses on troposphere modeling, time series analysis and homogenization for climate research.

Pavel Václavovic received his M.Sc. and Ph.D. degree in geodesy at the Czech Technical University in Prague in 2009 and 2017, respectively. Since 2011, he has worked at Geodetic Observatory Pecný with main research field focused on algorithms for precise point positioning with GNSS. He is a core developer of the G-Nut software library and end-user applications.

Kryštof Eben received his Ph.D. in mathematical statistics in 1986 from the Czech Academy of Sciences. He works in the Institute of Computer Science since 1991. His research interests are data assimilation, numerical weather models, and applications of mathematical statistics in energy meteorology.

Pavel Krč received his Master's degree at the Faculty of Mathematics and Physics of the Charles University in Prague in 2010. Currently, he is a Ph.D. student at the Czech Technical University and works in the Institute of Computer Science of the Czech Academy of Sciences. His research topics include atmospheric modeling, artificial intelligence, and data science.